# Density-dependent body-size distributions reveal populations state relative to carrying capacity

Man Qi[1]*, Jacques A. Deere[2,3], Isabel M. Smallegange[4], Roberto Salguero-Gomez[1]

1 Department of Biology, University of Oxford, 11a Mansfield Rd, Oxford OX1 3SZ, UK

2 School of Biosciences, University of Surrey, Stag Hill, Guildford, GU2 7XH, UK

3 Global Academy, University of Reading, Whiteknights, Reading, RG6 6EL, UK

4 School of Natural and Environmental Sciences, Newcastle University, Newcastle upon Tyne, NE1 7RU, UK

*Corresponding author: man.qi@biology.ox.ac.uk

**Open research statement**: Data and code for the mite experiment analysis can be found at https://github.com/ManQiEcology/Mite-Trait-Analysis---Density-dependence

**Abstract**

Phenotypic traits may provide accessible information about population dynamics, but how population-level trait distributions change along density-dependent trajectories remains poorly understood in populations with complex life cycles. Here, we quantified body-size distributions in three experimental populations of the bulb mite (*Rhizoglyphus robini*) as they increased from low density towards carrying capacity under constant environmental conditions and a fixed food supply. Population-level body-size distributions changed predictably but nonlinearly with relative density. Mean body size initially declined and subsequently increased towards carrying capacity, whereas variation and skewness showed broadly opposing patterns. Counterfactual decomposition showed that these changes reflected both shifts in population structure and changes in body size within developmental stages, with their relative contributions to mean body size varying along the density continuum. Stage-specific patterns also differed across development: later stages generally had smaller mean body sizes at higher densities, whereas early active juveniles showed the opposite pattern. Together, these results show that population-level trait distributions integrate concurrent changes in demographic structure and traits within developmental stages. They provide proof of principle that body-size distributions can inform density-dependent population state, while showing that their interpretation requires accounting for population structure, stage-specific trait change and nonlinear trait–density relationships.

**Keywords**: density dependence; population dynamics; resource limitation; trait ecology;

## Introduction

Understanding and predicting population dynamics is a central goal in ecology[1]. Population growth, persistence, and extinction emerge from the combinations of individual growth, reproduction and survival[2]. Accurate estimates of these vital rates therefore underpin population viability analyses[3], conservation planning[4], and forecasts of species responses to global change[5,6]. However, vital rates vary with population density[7,8], environmental conditions[9,10], and life-history processes[9]. Characterising this variation requires repeated observations across broad demographic and environmental gradients[11]. Such data typically require individuals to be identified and tracked through time, making their collection technically challenging and labour-intensive. Consequently, long-term individual-based demographic datasets suitable for predicting population dynamics remain available for relatively few populations[6,9,11].

Several complementary approaches are available for understanding and forecasting population change. Population viability analyses (PVAs) project population trajectories by modelling stage-specific growth, reproduction and survival from demographic observations[3]. Early warning signals (EWSs), by contrast, detect signals of impending population collapse from temporal changes in population-level variables such as abundance[12,13]. Both approaches, however, have substantial data requirements. PVAs require demographic observations spanning sufficient variation in population density and environmental conditions to characterise vital-rate responses[11], whereas EWSs generally require long, continuous time series[12,13]. Incorporating phenotypic traits such as body size can improves the predictive performance of EWSs[14], but the processes linking trait change to population dynamics remain poorly understood[14-17]. Understanding these links is necessary to determine what demographic information phenotypic traits can provide about changing populations.

57 Physiologically structured population models provide a complementary mechanistic
58 framework by linking individual physiology to demographic processes and population
59 dynamics[18-21]. For example, dynamic energy budget integral projection models (DEB-IPMs)
60 link energy acquisition and allocation to size-dependent growth, reproduction and population
61 structure[20]. By describing demographic rates through biologically interpretable physiological
62 processes, such models can reduce reliance on extensive individual-level demographic
63 observations[22]. A complementary empirical challenge is to identify readily measurable traits
64 that integrate these underlying processes and thereby contain information about population
65 change.

66 Phenotypic traits may provide readily measurable information about the processes
67 underlying population change. They occupy an intermediate position between individual-level
68 processes and population dynamics[23,24]. Body size is particularly informative because it reflects
69 the cumulative outcomes of intraspecific competition, resource availability, energy allocation
70 and life-history stage, while also being associated with growth, reproduction and survival[20].
71 Body-size distributions may therefore retain a phenotypic signature of the ecological and
72 demographic processes shaping population dynamics[20,23,25]. Recent advances in remote sensing,
73 computer vision and automated phenotyping increasingly allow body size to be quantified
74 rapidly across individuals and populations[25-27]. This combination of biological relevance and
75 measurability makes body size a promising trait for evaluating how phenotypic change reflects
76 population dynamics.

77 Density dependence provides an ecological link between population dynamics and
78 body size. Here, we define population state as a population's position along the density-
79 dependent continuum, quantified by relative population density ($N$/K), where $N$ is population
80 density and K is carrying capacity. As populations increase towards carrying capacity under
81 constant environmental conditions, increasing intraspecific competition can alter resource

82 availability, energy allocation, growth, reproduction and survival[20,28]. These processes can also
83 alter body size, generating systematic body-size responses along the density continuum[7,29,30]
84 (Box 1). Previous work has shown predictable density-dependent body-size responses in
85 unstructured populations[30]. Whether such relationships persist in stage-structured populations
86 is less clear because population-level body-size distributions can change through both shifts in
87 population structure and changes in body size within stages. These interacting sources of
88 variation may generate complex, potentially nonlinear relationships between population
89 density and body-size distributions.

90 Here, we tested how body-size distributions change along a density-dependent
91 population trajectory using experimental populations of the bulb mite *Rhizoglyphus robini*, a
92 species with a complex life cycle. We first asked whether population-level body-size
93 distributions change predictably as populations increase from low density towards carrying
94 capacity. We then examined how these population-level responses arise by separating the
95 contributions of changes in population structure from changes in body size within
96 developmental stages. Finally, we tested how the direction and magnitude of body-size
97 responses differ among developmental stages. Together, these analyses determine how
98 population structure and stage-specific body-size responses shape population-level trait
99 distributions along the density continuum, providing a proof of principle for evaluating their
100 potential to inform population state.

**Box 1. Density dependence links body size to population dynamics**

Density dependence can generate predictable relationships between individual body size and population density in unstructured populations under constant environmental conditions. Panel A illustrates the expected body size–density relationship. Following a demographic disturbance, reduced population density relaxes intraspecific competition and increases per-

capita resource availability, allowing surviving individuals to attain larger body sizes. As the population recovers towards carrying capacity, increasing competition can reduce body size. Panel B relates positions along this body size–density relationship to realised population growth rate, illustrating how body-size responses may contain information about a population's position along a density-dependent trajectory.

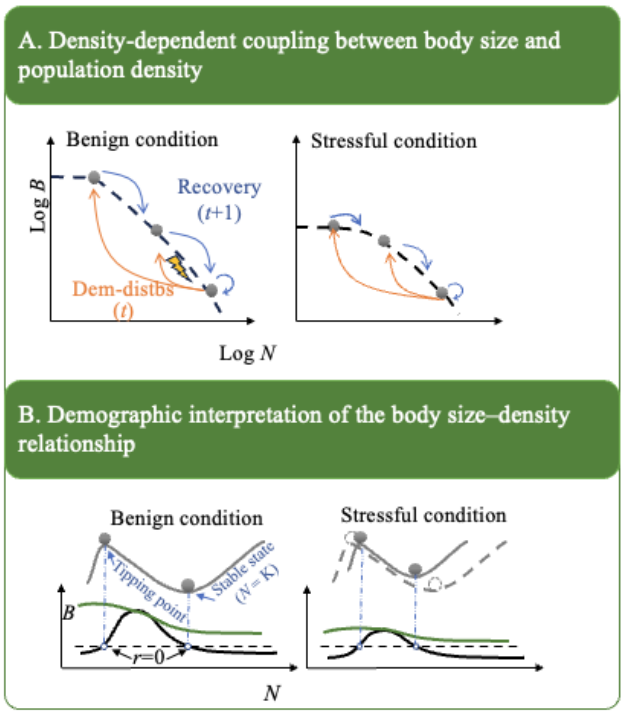


**Density-dependent coupling between body size (*B*) and population density (*N*) under constant environmental conditions.** Following a demographic disturbance, reduced population density relaxes intraspecific competition and increases per-capita resource availability, potentially allowing surviving individuals to attain larger body sizes. As population density recovers towards carrying capacity (*K*), competition intensifies and body size may decline. The resulting log*B*–log*N* relationship represents the expected outcome of density-dependent feedbacks in an unstructured population with a stable equilibrium. Environmental stress can alter both attainable body size and the strength of the body size–density relationship. Modified from Qi et al. (2026)[30].

**Demographic interpretation of the body size–population density relationship.** Under constant environmental conditions, positions along the log*B*–log*N* relationship correspond to different realised population growth rates (*r*, black curves). At low density, *r* may initially increase with population density when positive density dependence occurs. At higher densities, negative density dependence reduces *r*, which approaches zero as the population approaches carrying capacity (*K*). Meanwhile, body size (*B*) may decline as increasing density intensifies intraspecific competition. The joint responses of *B* and *r* to population density therefore illustrate how body-size change can accompany progression along a density-dependent population trajectory.

## Results

We analysed three replicate populations of the bulb mite *R.robini* from a one-year laboratory experiment[31] conducted under constant environmental conditions and a fixed daily

105 food supply. Population density increases naturally from low density towards carrying capacity,
106 providing a continuous density-dependent population trajectory. At repeated censuses, we
107 quantified the abundance of each developmental stage and randomly sampled individuals from
108 each developmental stage for body-size measurements. We first quantify population-level
109 body-size distributions (mean, coefficient of variation and skewness) along this trajectory. We
110 then separate their changes into contributions from population structure and within-stage body-
111 size change, before examining body-size responses within individual developmental stages.

112 All three populations exhibit logistic population growth and progress from low density
113 towards carrying capacity (Fig. 1a,b). Realised population growth rate ($r$) initially increases
114 with relative population density before declining towards zero as populations approach
115 carrying capacity (Fig. 1a). Population structure also changes systematically along the density
116 continuum (Fig. 1c). The proportion of eggs broadly follows the pattern in realised population
117 growth rate, whereas the proportion of juveniles shows an opposing pattern. In contrast, the
118 proportion of adults remains comparatively stable. Thus, increasing relative population density
119 is accompanied by marked changes in population structure, providing the demographic context
120 for interpreting population-level body-size distributions.

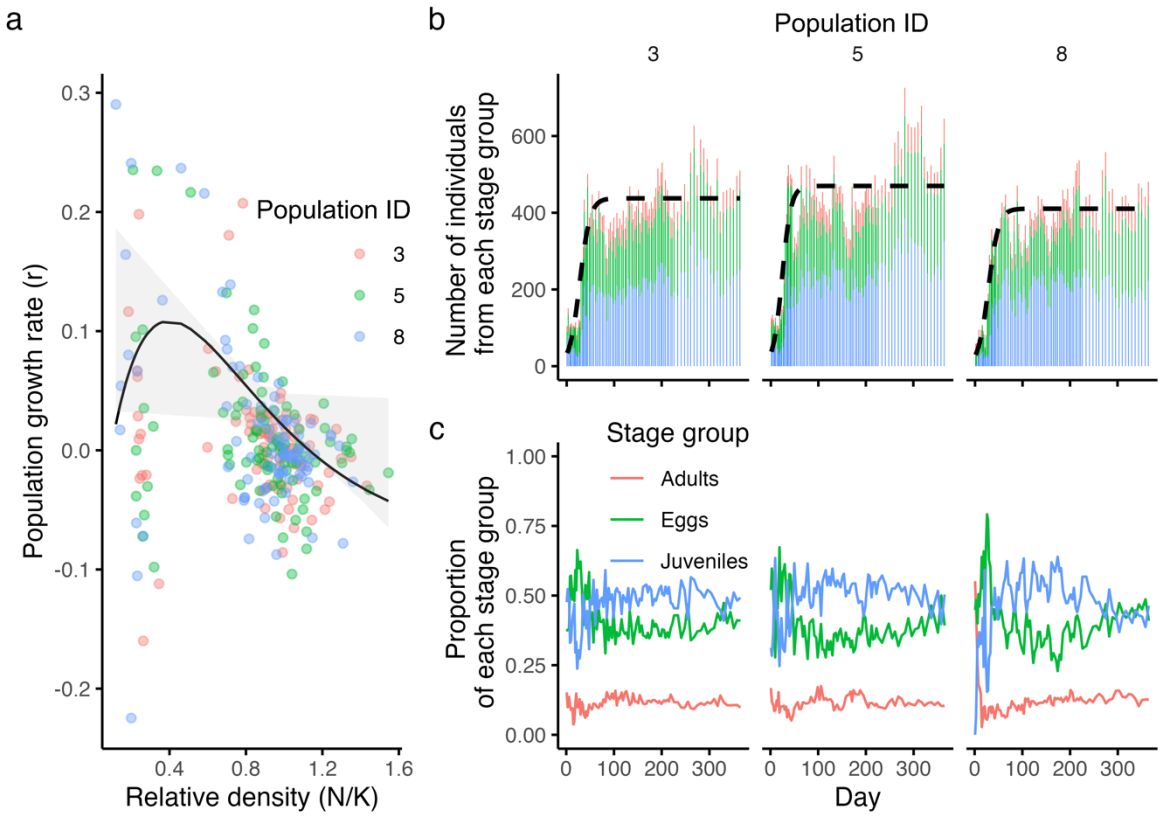


**Fig. 1 Experimental bulb mite populations progress from low density towards carrying capacity with concurrent changes in population structure. a,** Relationship between realised population growth rate ($r$) and relative population density ($N/K$) across three replicate populations. Points represent daily realised population growth rates estimated from interpolated abundance trajectories. The solid line shows the fitted generalized Ricker model and grey shading indicates the 95% confidence interval. **b,** Population abundance through time for each replicate population. Stacked bars show the abundance of eggs, juveniles and adults. Dashed lines show fitted logistic growth curves used to estimate carrying capacity ($K$). **c,** Proportional abundance of eggs, juveniles and adults through time in each replicate population.

Population-level body-size distributions change predictably but nonlinearly along the density continuum (Fig. 2a–c). Mean body size declines from low relative density to a minimum at approximately half carrying capacity, before increasing and stabilising towards carrying capacity (GAM, $p < 0.001$; Fig. 2a). The coefficient of variation (CV) and skewness

show broadly opposite patterns. Both increase from low to intermediate relative density and subsequently decline towards carrying capacity (both $p < 0.001$; Fig. 2b,c). Replicate populations differ slightly in mean body size, but show consistent density-dependent patterns in CV and skewness (Appendix S1: Table S1). Thus, body-size distributions vary systematically along the density continuum, but no single population-level body-size metric changes monotonically with relative population density.

Population-level body-size distributions change through contributions from both population structure and within-stage body-size change (Fig. 2d–f). The decomposition separates changes arising from shifts in the relative abundance of developmental stages from those arising when body size changes within stages. Both components contribute to changes in all three population-level body-size metrics, but their relative contributions differ among metrics and across the density continuum. For mean body size, the contribution of population structure declines significantly with increasing relative density (GAM: edf = 1.00, $F = 9.71$, $p = 0.002$; Fig. 2d; Appendix S1: Table S2), while the contribution of within-stage body-size change increases correspondingly. In contrast, the relative contributions of the two components to changes in CV and skewness do not vary significantly with relative density (CV: edf = 2.43, $F = 2.49$, $p = 0.102$; skewness: edf = 1.00, $F = 1.56$, $p = 0.213$; Fig. 2e,f). Thus, population-level body-size distributions integrate changes in both demographic structure and body size within developmental stages, with their relative importance for mean body size shifting along the density continuum.

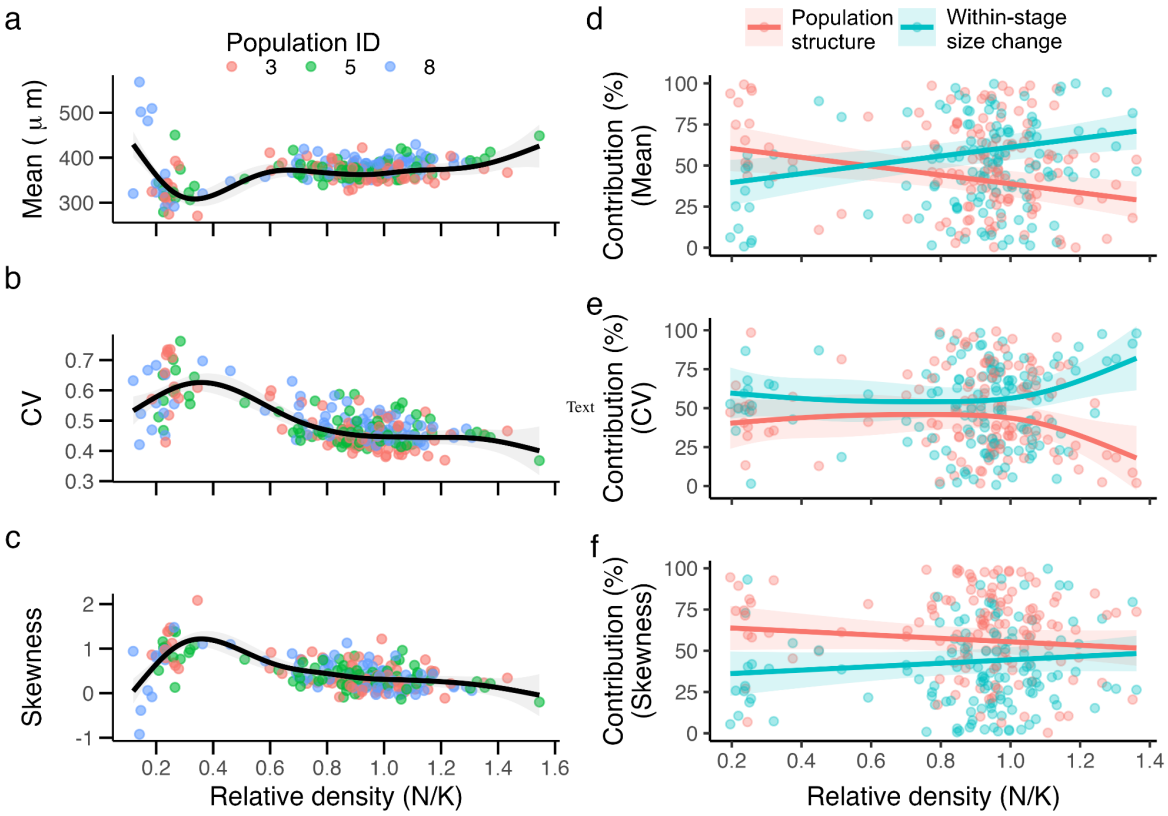


155

156 **Fig. 2 Population-level body-size distributions change nonlinearly along the density**
157 **continuum through contributions from population structure and within-stage body-size**
158 **change.** **a–c**, Relationships between relative population density (*N/K*) and population-level a,
159 mean body size, **b**, coefficient of variation (CV) and **c**, skewness. Points represent census-level
160 observations across three replicate populations. Black lines show generalized additive model
161 (GAM) fits and grey shading indicates 95% confidence intervals. **d–f**, Symmetric Shapley
162 decomposition of changes in **d**, mean body size, **e**, CV and **f**, skewness into contributions from
163 changes in population structure and within-stage body size. Points represent estimates from
164 consecutive moving-window comparisons. Lines show GAM fits and shading indicates 95%
165 confidence intervals. Contributions are expressed as percentages of the total absolute change
166 in each body-size metric.

Density-dependent changes in mean body size differ markedly among developmental stages (Fig. 3). Mean body size changes significantly with relative population density in every developmental stage (all GAMs, $p < 0.05$; Appendix S1: Table S3), but the direction and magnitude of these responses vary across ontogeny. Adults show the strongest declines in mean body size with increasing relative density, while quiescent juvenile stages show weaker negative responses. In contrast, active juvenile stages generally increase in mean body size from low to intermediate relative density before stabilising towards carrying capacity. Egg size changes comparatively little across the density continuum. Stage-specific correlations with population abundance support these contrasting responses, with later developmental stages showing predominantly negative associations and early stages showing weaker or positive associations (Appendix S1: Fig. S3). Thus, the direction of density-dependent body-size change shifts across development, from generally positive responses in early active juvenile stages to negative responses in later developmental stages.

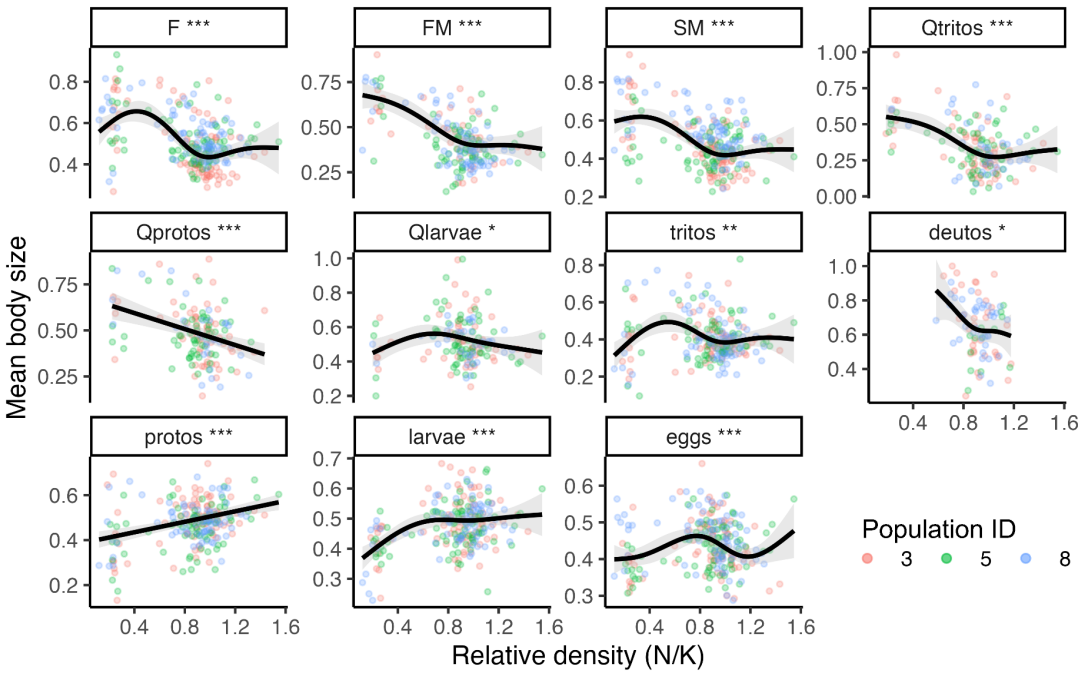

**Fig. 3 Density-dependent changes in mean body size differ across developmental stages.** Relationships between relative population density (*N/K*) and stage-specific mean body size in bulb mite (*Rhizoglyphus robini*) populations. Points represent census-level observations across three replicate populations, with colours indicating population identity. Black lines show generalized additive model (GAM) fits and grey shading indicates 95% confidence intervals. GAMs are fitted separately for each developmental stage, with significance of the smooth term indicated in each panel (∗ $p$<0.05; ** $p$ < 0.01; ∗∗∗ $p$<0.001). F – female, FM – fighter male, SM – scrambler male, Qtritos – Quiescent tritonymph, Qproto – Quiescent protonymph, Qlarvae – Quiescent larvae, tritos – tritonymph, deuto – deutonymph, protos – protonymph.

Density-dependent changes in within-stage body-size variation are less consistent across developmental stages than changes in mean body size (Fig. 4). The coefficient of variation (CV) changes significantly with relative population density in most developmental stages, but the direction of these responses differs among stages. Adults and quiescent juvenile stages generally show increasing CV with relative density, whereas active juvenile stages generally show declining CV (Fig. 4; Appendix S1: Table S3). In contrast, skewness generally shows no significant relationship with relative population density across developmental stages (Appendix S1: Fig. S4). Thus, density-dependent changes within developmental stages are expressed most consistently in mean body size, whereas variation is more stage-specific and distributional asymmetry is less density dependent.

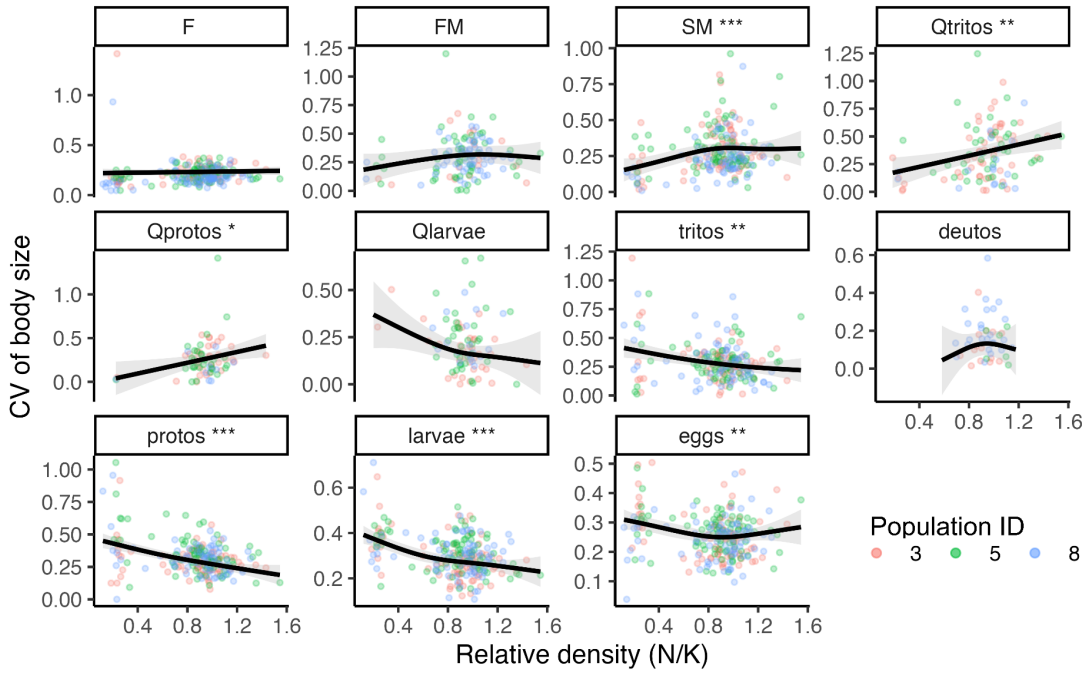


**Fig. 4 Density-dependent changes in body-size variation differ among developmental stages.** Relationships between relative population density (*N/K*) and the stage-specific coefficient of variation (CV) in body size in bulb mite (Rhizoglyphus robini) populations. Points represent census-level observations across three replicate populations, with colours indicating population identity. Black lines show generalized additive model (GAM) fits and grey shading indicates 95% confidence intervals. GAMs are fitted separately for each developmental stage, with significance of the smooth term indicated in each panel (∗ $p$<0.05; ** $p$ < 0.01; ∗∗∗ $p$<0.001). F – female, FM – fighter male, SM – scrambler male, Qtritos – Quiescent tritonymph, Qproto – Quiescent protonymph, Qlarvae – Quiescent larvae, tritos – tritonymph, deuto – deutonymph, protos – protonymph.

## Discussion

How population-level trait distributions change along density-dependent population trajectories remains poorly understood in populations with complex life cycles. In stage-structured populations, changes in trait distributions can arise from shifts in population structure, changes in traits within developmental stages, or both, complicating their

demographic interpretation. Here, we show that population-level body-size distributions change predictably but nonlinearly as bulb mite populations progress from low density towards carrying capacity. Counterfactual decomposition shows that these changes reflect contributions from both shifts in population structure and within-stage body-size change, with their relative contributions to changes in mean body size varying along the density continuum. Developmental stages also differ in their patterns of body-size change: mean body size generally increases with relative density in early active juveniles but decreases in later developmental stages. Together, these findings show that resolving changes in population structure and traits within developmental stages is key to interpreting how population-level trait distributions relate to density-dependent population dynamics.

The nonlinear changes in population-level body-size distributions reflect concurrent changes in population structure and body size within developmental stages. From low density to approximately half carrying capacity, the proportion of eggs increases while the proportion of juveniles decreases (Fig. 1c). Because eggs (size range: 103-253 μm) are substantially smaller than juveniles (307-605 μm) and adults (304-1050), this shift in population structure is consistent with the concurrent decline in population-level mean body size and increases in CV and skewness (Fig. 2a–c). Changes in body size within developmental stages may further modify these patterns. For example, the relatively large body sizes observed in several later developmental stages at intermediate densities may contribute to greater variation and asymmetry in the population-level distribution (Fig. 3). From approximately half carrying capacity towards carrying capacity, the proportion of eggs declines while the proportion of juveniles increases, coinciding with increasing population-level mean body size and declining CV and skewness. At the same time, mean body size declines in several later developmental stages, potentially moderating the increase in population-level mean body size. The resulting

240 population-level trajectory therefore reflects the combination of changing stage composition
241 and changing body-size within stages.

242 Importantly, the biological interpretation of population-level mean body size changes
243 along the density continuum. At lower densities, changes in mean body size are more strongly
244 associated with shifts in population structure, whereas changes observed within developmental
245 stages become relatively more important towards carrying capacity (Fig. 2d). Both population
246 structure (Fig. 1c) and body size within developmental stages (Fig. 3) vary nonlinearly with
247 relative density, consistent with the nonlinear pattern observed in population-level body size
248 (Fig. 2a–c). This nonlinear body size–density relationship limits the interpretation of a single
249 body-size measurement. Similar trait values may occur at different relative densities and arise
250 from different combinations of population structure and within-stage body size. However,
251 when repeated trait measurements are available, the direction and magnitude of change along
252 the response curve may provide additional information about population state. For structured
253 populations, the trajectory of a trait distribution may therefore be more informative than its
254 value at a single time point.

255 Body-size changes with relative density differ markedly among developmental stages,
256 showing that population-level patterns mask contrasting changes across the life cycle. Adults
257 and later juvenile stages generally show smaller mean body size at higher relative density,
258 consistent with negative size–density relationships reported in other stage- or age-structured
259 populations[5,28]. In contrast, early active juvenile stages show larger mean body size at higher
260 relative density (Fig. 3). One possible explanation for the stronger negative associations in later
261 stages is the cumulative effect of resource limitation across development. Under a fixed food
262 supply, increasing population density reduces per-capita food availability, which could
263 constrain growth over successive developmental stages. The larger body sizes observed in
264 some early juvenile stages could instead reflect selective survival[32,33], whereby smaller

individuals are less likely to persist to measurement, or parental effects on offspring size[34,35]. These explanations are not mutually exclusive, and distinguishing among them will require simultaneous measurements of body size, stage-specific vital rates and resource acquisition across the density continuum.

Although we focus on density-dependent changes in body size, population density covaries with other components of population development. Population structure is particularly important because it changes concurrently with density and cannot be experimentally separated from density in our populations. We therefore treat density and population structure as interdependent components of the population trajectory under constant environmental conditions. Initial population structure can strongly influence short-term population trajectories, generating transient dynamics that differ from longer-term population behaviour. In the absence of further perturbation, the influence of initial demographic structure is expected to diminish as population converge towards a stable demographic state[36]. As populations increase towards carrying capacity under a fixed food supply, per-capita resource availability also declines, increasing the potential for density dependent competition. Consistent with this progression, all three replicate populations converge towards similar carrying capacities while showing systematic changes in population structure and body-size distributions (Figs. 1–3). This distinction is important for comparative studies, where sufficient time should be allowed for transient effects of initial demographic conditions to diminish before trait–density relationships are interpreted as characteristic of a population. Mechanistic approaches that link resource acquisition and allocation to stage-specific demography, such as DEB-IPMs[20], could further resolve how density, population structure and within-stage trait change are coupled during population development.

Our results provide a proof of principle that body-size distributions contain information about density-dependent population development in a stage-structured population. This

information is not captured by a simple relationship between body size and population density. Instead, population-level trait distributions integrate changes in population structure and body size within developmental stages, and these components vary differently along the density continuum. Applying this approach to natural populations will require establishing how these relationships vary among species and environmental conditions, particularly where resource availability and other environmental drivers change through time. Comparative studies that combine repeated trait measurements with population structure and demographic data will be important for testing when trait trajectories provide reliable information about population state. More broadly, our findings show that interpreting population-level trait distributions requires considering not only how traits change, but also how the demographic composition of the population changes with them.

## Online methods

*Bulb mite experiment*

We analysed body-size and demographic data from three undisturbed control populations of the bulb mite *Rhizoglyphus robini* established as part of a previously published long-term laboratory experiment[31]. Populations were kept in 20 mm diameter, flat-bottomed glass tubes. Each population was initiated with 50 randomly selected adults from a laboratory stock population and maintained in enclosed populations under constant environmental conditions (25 °C, >70% relative humidity)[35]. Each population was fed with a fixed daily food supply of 0.5 mg yeast per day.

To reduce founder effect, the founder mites were removed after 15 days, by which time the next generation had matured. Founder mites were much larger than mites from subsequent generations and so it was easy for them to be distinguished. After initialization, no harvesting or other external disturbance was applied to the populations analysed in this study. Thereby,

314 population density increased naturally from low density towards carrying capacity following
315 logistic growth. Population stabilized in population size at about 40 days after initialization and
316 were monitored for 365 days after initialization, approximately 10 generations of bulb mites[31].

317 Individuals in every developmental stage were counted twice weekly during the first 230 days
318 and weekly thereafter. Photos were taken at 15× magnification of up to 10 individual adult
319 females, fighters, scrambles and preimaginal quiescent tritonymphs. The body length of mites
320 (with mouthparts) on each photo was measured to the nearest 0.1 μm. For the next 135 days of
321 the experiment, mites were measured every other week (more details can be found in
322 Smallegange & Deere (2014)[31]).

323 *Statistical analyses*

324 *Population dynamic analysis*

325 To quantify population dynamics along the density continuum as populations increase from
326 low density to carrying capacity, we fitted logistic population growth curves to observed
327 population abundance over time. We also calculated realised population growth rate of each
328 population and analysed their relationship with relative population density to carrying capacity.
329 Relative population density was calculated by dividing the observed population abundance (*N*)
330 by the estimated carrying capacity (K) obtained from the fitted logistic growth model.

331 Firstly, we estimated the carrying capacity (K) of each population and divided the population
332 states by population abundance relative to carrying capacity. Carrying capacity was estimated
333 by fitting logistic population growth curves to the observed time series of abundance (*N*)
334 separately for each replicate population. Population equilibrium was defined as the point at
335 which fitted abundance exceeded 99% of the estimated carrying capacity.

Secondly, to characterize realized density dependence, we estimated daily population growth rates from observed times series of abundance. Population abundances, originally recorded every three to seven days over the 365-day experiment, were linearly interpolated to daily values, from which daily finite growth rate ($\lambda_t$) were calculated as $\lambda_t = N_{t+1}/N_t$, realised population growth rates were then calculated as $r_t = log\ (\lambda_t)$. Interpolated daily abundance values were used only to estimate the realised growth-rate trajectory.

Thirdly, to understand how population growth rate changes along the density continuum, we fit the realised population growth rate to relative population density to carrying capacity with a generalized Ricker model and Beverton-Holt model[37]. Because observations of population growth rate were unevenly distributed along the density gradient, analyses were weighted to avoid over-representation of densities near carrying capacity. Population sizes were divided into 20 equally spaced abundance bins, and each observation received a weight equal to the inverse of the number of observations within its bin. Weighted nonlinear least squares was then used to fit two models describing the relationship between realized population growth rate ($r$) and population size ($N$). The first was a generalized Ricker model designed to capture negative density dependence: $r = a(N + c)e^{-b(N+c)} + d)$, where $N$ is population size, and parameters $a$, $b$, $c$, and $d$ govern the shape and peak of the curve. The second was a modified Beverton-Holt model[37] designed to capture both Allee effects and negative density dependence: $r = \frac{a(N+c)^{d-1}}{1+b(N+c)^d} + e$, where parameters $a$, $b$, c, $d$, and $e$ allow flexible curvature including an internal peak. Nonlinear least squares regression was performed using the nlsLM function from the '*minpack.lm'* package in R v4.3.2[38]. Model performance was compared using root mean squared error (RMSE).

*Population-level body size distribution analysis along density continuum*

To quantify changes in population-level body-size distributions along the density continuum, we calculated the mean, coefficient of variation (CV), and skewness of body size at each census by pooling all measured individuals across developmental stages within each population. We analysed the relationship between each body-size metric and relative population density using generalized additive models (GAMs): $y = \beta_{tube} + s(q)$, where $y$ is the body-size metric, $q$ is relative population density, $s(q)$ is a penalized regression spline describing the nonlinear response to density, and population identity was included as a fixed effect to account for consistent differences among replicate populations. Models were fitted using restricted maximum likelihood (REML) using the 'mgcv' package in R (v4.3.2)[38].

To quantify the relative contributions of population structure and body-size change to shift in the population-level body size distribution along the density continuum, we performed a symmetric Shapley counterfactual decomposition[39]. Specifically, for each pair of consecutive censuses, we constructed four virtual populations with combination of population structure and stage-specific body-size distributions from each of the pairwise censuses: 1) Baseline population — population structure and stage-specific body-size distributions from the earlier census; 2) Structure-only population — population structure from the later census combined with stage-specific body-size distributions from the earlier census; 3) Size-only population— population structure from the earlier census combined with stage-specific body-size distributions from the later census; 4) Observed population — population structure and stage-specific body-size distributions from the later census. We further quantified the relative contributions of population structure and within-stage body-size change using Shapley counterfactual decomposition. This decomposition separates population-level body-size change associated with changing stage composition from change associated with differences in body size within stages. The incremental effect of population structure on a specific metric

of population-level body size distribution was calculated as $\Delta s = \frac{(M_s - M_0) + (M_{sp} - M_p)}{2}$, where $M_0$ is the body size metrics of baseline population, $M_s$ is that of structure-only population, $M_p$ is that of the change-only population, and $M_{sp}$ is that of the observed population. Similarly, The incremental effect of within-stage body-size change on a specific metric of population-level body size distribution was calculated as $\Delta p = \frac{(M_p - M_0) + (M_{sp} - M_s)}{2}$. The contribution of each component was expressed as a percentage of the total absolute change of body size metrics $contribution_j = 100 \times \frac{|\Delta j|}{|\Delta p| + |\Delta s|}$, where $j$ is $s$ or $p$. This symmetric formulation avoids dependence on the order in which population structure and body-size change are introduced and provides an unbiased partitioning of density-dependent changes in population-level body-size distributions.

Since our dataset has a limited number of body size observations at each census, to increase the number of body-size observations available for each decomposition while retaining local changes along the density continuum, we used a moving window of five censuses with a step of two censuses. This configuration was selected using a sensitivity analysis across alternative window lengths and step sizes (Appendix S1: Fig. S1-S2). Symmetric Shapley counterfactual decomposition was done between pairs of consecutive moving windows. For each moving window, population structure was quantified by summing the abundance of every developmental stage across all censuses within the window and expressing these abundances as stage proportions. Stage-specific body-size distributions were estimated independently by pooling all body-size measurements belonging to the same developmental stage within the corresponding moving window. Population-level body-size distributions of virtual populations were generated in two sequential steps. First, a standardized synthetic population containing 2,000 individuals was constructed according to the assigned composition of developmental stages. Second, each simulated individual was assigned a body size by randomly sampling,

with replacement, from the empirical body-size distribution of its corresponding developmental stage. Pooling all simulated individuals as the virtual population produced a population-level body-size distribution from which the mean, coefficient of variation and skewness were calculated. This simulation was repeated 1,000 times for every moving window, and average values across simulations were retained.

To test whether population structure or body size change contribute more to shift in body size distribution along density continuum, we apply the generalized additive models (GAMs) $contribution_j = \beta_{tube} + s(q)$, where $contribution_j$ is the contribution from population structure or body size change, $q$ is the mean relative population density of censuses within each moving window, $s(q)$ is a penalized regression spline describing the nonlinear response to density. Population identity was included as a fixed effect to account for consistent differences among replicate populations. Models were fitted using restricted maximum likelihood (REML) using the 'mgcv' package in R (v4.3.2)[38].

*Developmental-stage specific response of body size along density continuum*

To identify how each developmental stage differs in density dependent response of body size body size was analysed separately for each developmental stage. Because absolute body size differs substantially among developmental stages, body size within each stage was first standardized to the range 0–1 using min–max scaling after removing extreme outliers (>3 interquartile ranges from the first or third quartile). This standardization preserved relative changes in body size within each developmental stage while enabling direct comparisons of density-dependent responses among stages. For each population census, the mean body size, coefficient of variation (CV), and skewness were calculated separately for every developmental stage. Generalized additive models (GAMs) were then fitted independently for each stage and body-size metric using relative population density ($q=N/K$) as a penalized regression spline and

population identity (tube) as a fixed effect: $metric_i = \beta_{tube} + s(q)$. Smoothing parameters were estimated by restricted maximum likelihood (REML). Because developmental stages differed markedly in sample size, analyses of skewness were restricted to stage–census combinations containing at least three individuals. Stages lacking sufficient observations were excluded from the corresponding analysis.


## Acknowledgements

This study was supported by MSCA fellowship (EP/Z00232X/1, awarded to MQ). IMS is supported by the Natural Environment Research Council (NERC) grant RES/0578/7398.


## References


1 Sutherland, W. J. *et al.* Identification of 100 fundamental ecological questions. *Journal of Ecology* **101**, 58-67, doi:10.1111/1365-2745.12025 (2013).

2 Caswell, H. *Matrix Population Models: Construction, Analysis, and Interpretation*. (Sinauer Associates, 2001).

3 Decker, D. J. *Challenges In The Conservation Of Biological Resources: A Practitioner's Guide*. (Taylor & Francis, 2019).

4 Engelen, A., Davis, K., Ellis, A. G. & Salguero-Gómez, R. Poaching exacerbates the effects of climate change on the long-term viability of an endemic South African succulent plant species. *bioRxiv*, 2025.2001. 2020.633962 (2025).

5 van Benthem, K. J. *et al.* Trait–demography relationships underlying small mammal population fluctuations. *Journal of Animal Ecology* **86**, 348-358, doi:https://doi.org/10.1111/1365-2656.12627 (2017).

6 Paniw, M., Maag, N., Cozzi, G., Clutton-Brock, T. & Ozgul, A. Life history responses of meerkats to seasonal changes in extreme environments. *Science* **363**, 631-635, doi:doi:10.1126/science.aau5905 (2019).

7 Petraitis, P. S. The Role of Growth in Maintaining Spatial Dominance by Mussels (Mytilus Edulis). *Ecology* **76**, 1337-1346, doi:https://doi.org/10.2307/1940940 (1995).

8 Ricker, W. E. Stock and Recruitment. *Journal of the Fisheries Research Board of Canada* **11**, 559-623, doi:10.1139/f54-039 (1954).

9 Ozgul, A., Fichtel, C., Paniw, M. & Kappeler, P. M. Destabilizing effect of climate change on the persistence of a short-lived primate. *Proceedings of the National Academy of Sciences* **120**, e2214244120, doi:doi:10.1073/pnas.2214244120 (2023).

10 Sheth, S. N. & Angert, A. L. Demographic compensation does not rescue populations at a trailing range edge. *Proceedings of the National Academy of Sciences* **115**, 2413-2418, doi:doi:10.1073/pnas.1715899115 (2018).

11 Coulson, T., Mace, G. M., Hudson, E. & Possingham, H. The use and abuse of population viability analysis. *Trends in Ecology & Evolution* **16**, 219-221, doi:https://doi.org/10.1016/S0169-5347(01)02137-1 (2001).

12 Clements, C. & Ozgul, A. Indicators of transitions in biological systems. *Ecology Letters* **21**, doi:10.1111/ele.12948 (2018).

13 Scheffer, M. *et al.* Early-warning signals for critical transitions. *Nature* **461**, 53-59, doi:10.1038/nature08227 (2009).

14 Clements, C. F., Blanchard, J. L., Nash, K. L., Hindell, M. A. & Ozgul, A. Body size shifts and early warning signals precede the historic collapse of whale stocks. *Nature Ecology & Evolution* **1**, 0188, doi:10.1038/s41559-017-0188 (2017).

15 Arkilanian, A. A., Clements, C. F., Ozgul, A. & Baruah, G. Effect of time series length and resolution on abundance- and trait-based early warning signals of population declines. *Ecology* **101**, e03040, doi:https://doi.org/10.1002/ecy.3040 (2020).

16 Burant, J. B., Park, C., Betini, G. S. & Norris, D. R. Early warning indicators of population collapse in a seasonal environment. *Journal of Animal Ecology* **90**, 1538-1549, doi:https://doi.org/10.1111/1365-2656.13474 (2021).

17 Clements, C. F. & Ozgul, A. Including trait-based early warning signals helps predict population collapse. *Nature Communications* **7**, 10984, doi:10.1038/ncomms10984 (2016).

18 de Roos, A. M. in *Structured-Population Models in Marine, Terrestrial, and Freshwater Systems* (eds Shripad Tuljapurkar & Hal Caswell) 119-204 (Springer US, 1997).

19 Metz, J. A. J. & Diekmann, O.

20 Smallegange, I. M., Caswell, H., Toorians, M. E. & de Roos, A. M. Mechanistic description of population dynamics using dynamic energy budget theory incorporated into integral projection models. *Methods in Ecology and Evolution* **8**, 146-154 (2017).

21 Thunell, V., Gårdmark, A., Huss, M. & Vindenes, Y. Optimal energy allocation trade-off driven by size-dependent physiological and demographic responses to warming. *Ecology* **104**, e3967, doi:https://doi.org/10.1002/ecy.3967 (2023).

22 Smallegange, I. M. & Lucas, S. DEBBIES Dataset to study Life Histories across Ectotherms. *Scientific Data* **11**, 153, doi:10.1038/s41597-024-02986-x (2024).

23 Cerini, F., Childs, D. Z. & Clements, C. F. A predictive timeline of wildlife population collapse. *Nature Ecology & Evolution* **7**, 320-331, doi:10.1038/s41559-023-01985-2 (2023).

24 Ozgul, A., Coulson, T., Alan, R., Cameron, T. C. & Benton, T. G. Population Responses to Perturbations: The Importance of Trait-Based Analysis Illustrated through a Microcosm Experiment. *The American Naturalist* **179**, 582-594, doi:10.1086/664999 (2012).

25 Stone, T. C. & Davis, K. J. Using unmanned aerial vehicles to estimate body volume at scale for ecological monitoring. *Methods in Ecology and Evolution* **n/a**, doi:https://doi.org/10.1111/2041-210X.14457 (2024).

26 Rosen, A. *et al.* Modelling forest dynamics using integral projection models (IPMs) and repeat LiDAR. *bioRxiv*, 2025.2001.2006.631514, doi:10.1101/2025.01.06.631514 (2025).

27 Qi, M. *et al.* Biodiversity research requires more motors in air, water and on land. *Methods in Ecology and Evolution* **17**, 668-682, doi:https://doi.org/10.1111/2041-210x.70217 (2026).

28 Coulson, T. *et al.* Density dependent environments can select for extremes of body size. *Peer Community Journal* **2**, doi:10.24072/pcjournal.162 (2022).

29 Mrad, A. *et al.* Recovering the Metabolic, Self-Thinning, and Constant Final Yield Rules in Mono-Specific Stands. *Frontiers in Forests and Global Change* **3**, 62, doi:10.3389/ffgc.2020.00062 (2020).

30 Qi, M. *et al.* Density dependence buffers natural populations against multiple stressors. (2026).

31 Smallegange, I. M. & Deere, J. A. in *Advances in Ecological Research* Vol. 50 (eds Jordi Moya-Laraño, Jennifer Rowntree, & Guy Woodward) 145-169 (Academic Press, 2014).

32 Genovart, M., Oro, D. & Tenan, S. Immature survival, fertility, and density dependence drive global population dynamics in a long-lived species. *Ecology* **99**, 2823-2832, doi:https://doi.org/10.1002/ecy.2515 (2018).

33 Coulson, T. *et al.* Age, sex, density, winter weather, and population crashes in Soay sheep. *Science* **292**, 1528-1531, doi:10.1126/science.292.5521.1528 (2001).

34 Ozgul, A. *et al.* The Dynamics of Phenotypic Change and the Shrinking Sheep of St. Kilda. *Science* **325**, 464-467, doi:doi:10.1126/science.1173668 (2009).

35 Smallegange, I. M. Complex environmental effects on the expression of alternative reproductive phenotypes in the bulb mite. *Evolutionary Ecology* **25**, 857-873, doi:10.1007/s10682-010-9446-6 (2011).

36 Capdevila, P., Stott, I., Beger, M. & Salguero-Gómez, R. Towards a Comparative Framework of Demographic Resilience. *Trends in Ecology & Evolution* **35**, 776-786, doi:https://doi.org/10.1016/j.tree.2020.05.001 (2020).

37 Gascoigne, J. & Lipcius, R. Allee effects in marine systems. *Marine Ecology-progress Series - MAR ECOL-PROGR SER* **269**, 49-59, doi:10.3354/meps269049 (2004).

38 Team, R. C. (R Foundation for Statistical Computing, Vienna, Austria, 2024).

39 Shorrocks, A. F. Decomposition procedures for distributional analysis: a unified framework based on the Shapley value. *The Journal of Economic Inequality* **11**, 99-126, doi:10.1007/s10888-011-9214-z (2013).

Supplement

# Density-dependent body-size distributions reveal population state

Man Qi[1]*, Jacques A. Deere[2,3], Isabel M. Smallegange[4], Roberto Salguero-Gomez[1]

1 Department of Biology, University of Oxford, 11a Mansfield Rd, Oxford OX1 3SZ, UK

2 School of Biosciences, University of Surrey, Stag Hill, Guildford, GU2 7XH, UK

3 Global Academy, University of Reading, Whiteknights, Reading, RG6 6EL, UK

4 School of Natural and Environmental Sciences, Newcastle University, Newcastle upon Tyne, NE1 7RU, UK

*Corresponding author: man.qi@biology.ox.ac.uk

Appendix S1

## Selection of moving-window parameters

The moving-window parameters were selected by sensitivity analysis. Window lengths between three and eight censuses and step sizes between one and seven censuses were evaluated. For each parameter combination, the complete decomposition was repeated and generalized additive models were fitted to the resulting contribution curves.

Model uncertainty was quantified as the mean width of the 95% confidence intervals of the fitted GAM smooths across all body-size metrics and decomposition components. Increasing overlap between neighbouring windows reduced confidence-band width because adjacent windows shared a larger proportion of observations, whereas larger step sizes increased statistical uncertainty by reducing the overlap between successive comparisons (Supplementary Fig. S1).

The final moving-window configuration was selected as a compromise between statistical stability (requires smaller step size, longer window) and temporal independence (requires bigger step size, narrower window). A window length of five consecutive censuses with a step size of two censuses (i.e. w5 s2 in Figure S1, 60% overlap) produced stable contribution estimates while preserving sufficient differences between neighbouring windows to represent local changes along the density continuum (Supplementary Fig. S2). Qualitatively similar trends were obtained across a broad range of window configurations, indicating that the biological conclusions were robust to reasonable choices of moving-window parameters.

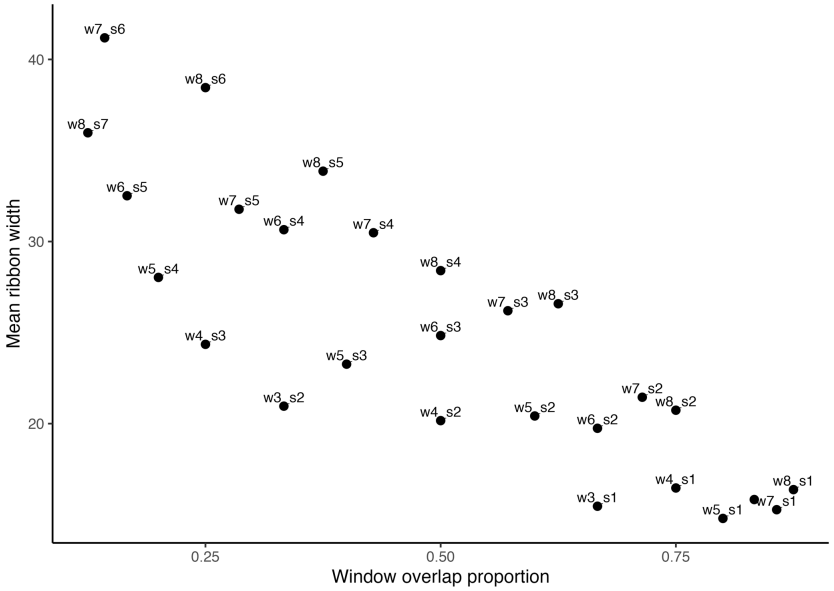


**Fig. S1** Trade-off between temporal overlap and statistical uncertainty in the moving-window decomposition. Relationship between the proportion of observations shared by consecutive moving windows and the mean width of the 95% confidence intervals of generalized additive models fitted to the estimated contributions of population structure and within-stage body-size change. Each point represents one moving-window configuration, labelled by its window length (*w*) and step size (*s*). Increasing overlap between neighbouring windows generally reduced uncertainty because adjacent windows shared more observations, whereas lower overlap increased temporal independence at the cost of greater sampling variance. Based on

this trade-off, a window length of five censuses with a step size of two censuses (60% overlap) was selected as a compromise between statistical stability and the ability to resolve local changes in population state.

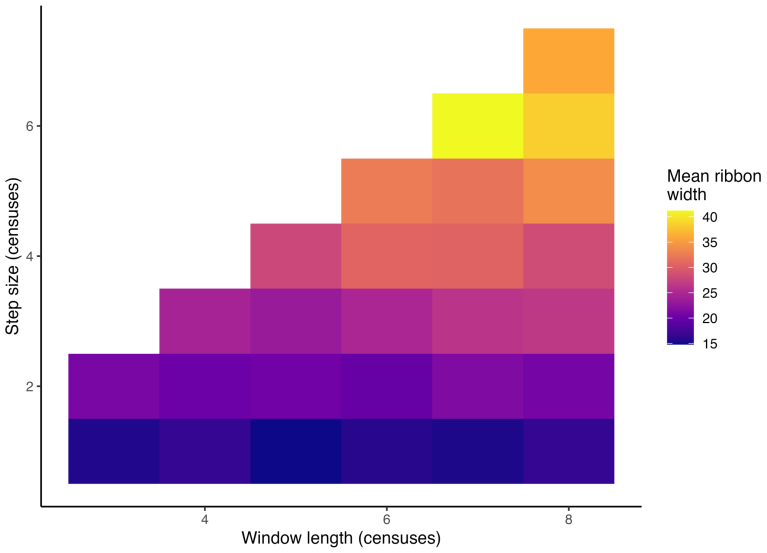


**Fig. S2** Sensitivity analysis of moving-window parameters used for counterfactual decomposition. Mean width of the 95% confidence intervals of generalized additive models (GAMs) fitted to the estimated contributions of population structure and within-stage body-size change for different combinations of moving-window length (number of consecutive censuses included in each window) and step size (number of censuses separating successive windows). Darker colours indicate narrower confidence intervals and therefore lower uncertainty in the estimated contribution curves. Increasing window length and overlap between successive windows generally reduced statistical uncertainty by increasing the number of observations contributing to each decomposition. This analysis was used to identify moving-window configurations that balanced statistical stability with temporal resolution.

## Correlations between stage-specific body size and population abundance

To explore how body size at different developmental stages was associated with population structure across the density gradient, we examined pairwise correlations between standardized stage-specific body sizes and population structure variables. Body size within each developmental stage was first standardized to a range of 0–1 using min–max scaling after removing extreme outliers (>3 interquartile ranges). Pairwise Spearman's rank correlation coefficients were then calculated between standardized stage-specific body sizes and population structure variables, including stage-specific abundances, total population abundance, and relative population density ($q$). Correlations were calculated using pairwise

complete observations. Statistical significance was evaluated using two-sided tests, and *p* values were adjusted for multiple comparisons using the Benjamini–Hochberg false discovery rate (FDR) procedure.

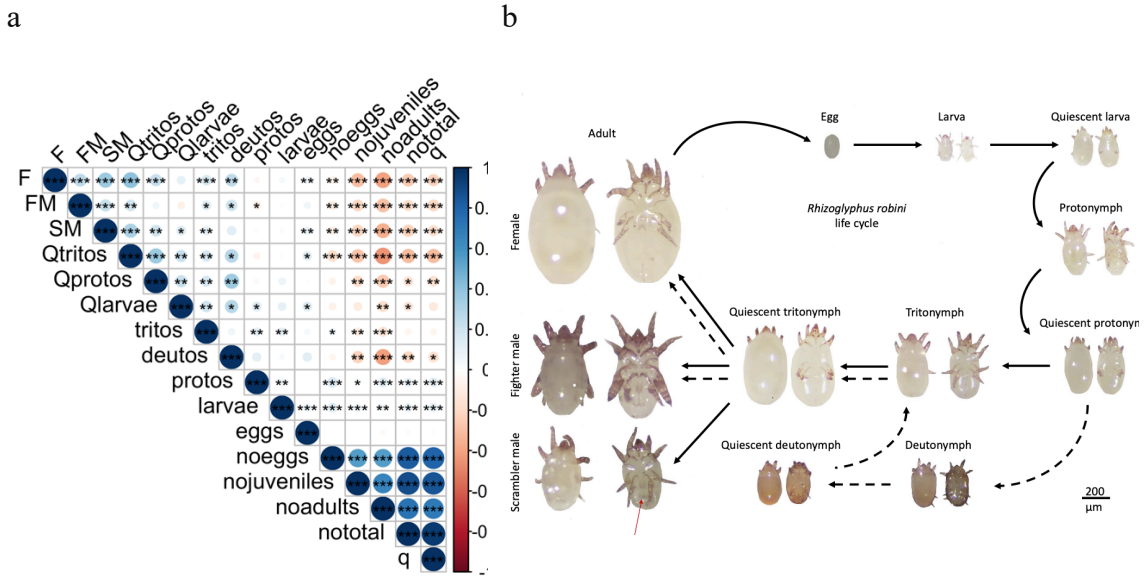


**Fig. S3 Correlations between stage-specific body size and population abundance support stronger density-dependent responses in later developmental stages. (a)** Spearman correlation coefficients between individual body size of each developmental stage and population abundance (*nototal*). Abundance of early-, mid- and late-stage groups (*noeggs*, *nojuveniles*, *noadults*) was introduced to identify stages causing higher density dependent response of body size. **(b)** Life cycle of bulb mite *Rhizoglyphus robini*[1]. F-Female, FM-Fighter male, SM-Scrambler male , Q means quiescent in Qtritos, Qprotos, and Qlarvae. $p<0.001$ (***), $p<0.01$ (**), $p<0.05$ (*).

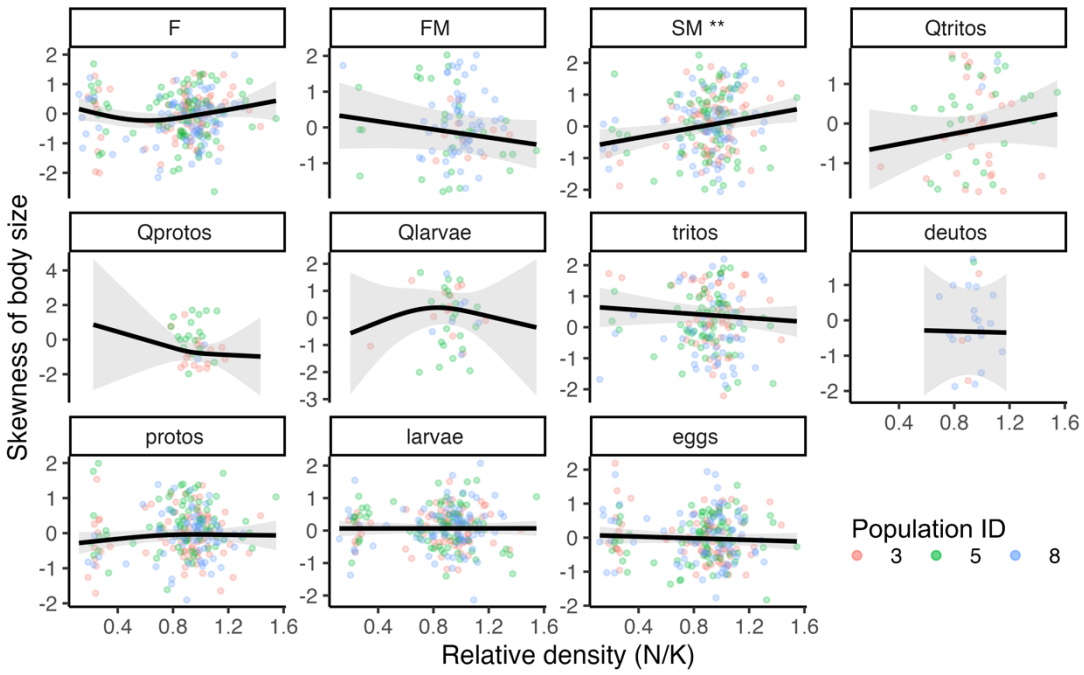


**Fig. S4 Skewness of body size distribution generally show no significant response to change in population density.** Relationships between relative population density (N/K) and stage-specific skewness of body-size distribution in bulb mite populations. Points represent census-level observations from three replicate populations (colours indicate tube identity). Black lines show generalized additive model (GAM) fits and grey shading indicates 95% confidence intervals. Density-dependent responses were analysed separately for each developmental stage, with significance of the smooth term indicated in the head title of each panel (∗ $p$<0.05; ** $p$ < 0.01; ∗∗∗ $p$<0.001; ns, not significant).

**Table S1** Generalized additive models describing shift in population-level body size distribution along the density continuum. Generalized additive models (GAMs) were fitted separately for mean body size, coefficient of variation (CV), and skewness. Relative population density (q) was modelled as a penalized regression spline to test whether each body-size metric varied along the density continuum, while replicate population identity (represented by tube number) was included as a fixed effect to account for differences among replicate populations.

| Response | Model term | Estimate | edf | F | p | Adjusted $r^2$ | Deviance explained (%) |
|---|---|---|---|---|---|---|---|
| Mean | Intercept | 363.08 | – | – | <0.001 | 0.312 | 33.9 |
| | Tube 5 | 7.65 | – | – | 0.078 | | |
| | Tube 8 | 15.83 | – | – | <0.001 | | |
| | s(q) | – | 7.7 | 10.3 | <0.001 | | |
| CV | Intercept | 0.478 | – | – | <0.001 | 0.533 | 54.8 |
| | Tube 5 | 0.006 | – | – | 0.436 | | |
| | Tube 8 | 0.016 | – | – | 0.05 | | |
| | s(q) | – | 6.16 | 37.96 | <0.001 | | |
| Skewness | Intercept | 0.444 | – | – | <0.001 | 0.418 | 44 |
| | Tube 5 | −0.014 | – | – | 0.754 | | |
| | Tube 8 | −0.004 | – | – | 0.932 | | |
| | s(q) | – | 7.32 | 21.35 | <0.001 | | |

**Table S2** Generalized additive models describing density-dependent changes in the contribution of population structure to body-size distribution metrics. Because the contribution of body-size change was calculated as the complement of population structure (size change = 100 − population structure), only models for population structure are reported. q-relative population density.

| Response | Model term | Estimate | edf | F | *p* | Adjusted $r^2$ | Deviance explained (%) |
|---|---|---|---|---|---|---|---|
| Mean | Intercept | 41.89 | – | – | <0.001 | 0.103 | 12.3 |
| | Tube 5 | 13.58 | – | – | 0.014 | | |
| | Tube 8 | 13.98 | – | – | 0.012 | | |
| | s(q) | – | 1 | 9.71 | 0.002 | | |
| CV | Intercept | 42.44 | – | – | <0.001 | 0.067 | 9.87 |
| | Tube 5 | 5.30 | – | – | 0.33 | | |
| | Tube 8 | 12.47 | – | – | 0.022 | | |
| | s(q) | – | 2.43 | 2.49 | 0.102 | | |
| Skewness | Intercept | 56.64 | – | – | <0.001 | 0.007 | 2.99 |
| | Tube 5 | 6.96 | – | – | 0.19 | | |
| | Tube 8 | 7.31 | – | – | 0.169 | | |
| | s(q) | – | 1 | 1.56 | 0.213 | | |

**Table S3 Generalized additive models describing shift in body size distribution of stage groups along the density continuum.** Generalized additive models (GAMs) were fitted separately for mean body size, coefficient of variation (CV), and skewness. Relative population density ($q$) was modelled as a penalized regression spline to test whether each body-size metric varied along the density continuum, while replicate population identity (represented by tube number) was included as a fixed effect to account for differences among replicate populations.

| Metrics | Stage group | Model term | Estimate | edf | F | p | Adjusted $r^2$ | Deviance explained (%) |
|---|---|---|---|---|---|---|---|---|
| Mean body size | Adults | Intercept | 0.47 | – | – | <0.001 | 0.391 | 40.5 |
| | | Tube 5 | 0.01 | – | – | 0.713 | | |
| | | Tube 8 | 0.05 | – | – | 0.002 | | |
| | | s(q) | – | 3.66 | 38.70 | <0.001 | | |
| | Q_juveniles | Intercept | 0.44 | – | – | <0.001 | 0.163 | 18.1 |
| | | Tube 5 | 0.00 | – | – | 0.998 | | |
| | | Tube 8 | 0.03 | – | – | 0.138 | | |
| | | s(q) | – | 3.19 | 12.90 | <0.001 | | |
| | Active juveniles | Intercept | 0.47 | – | – | <0.001 | 0.242 | 25.9 |
| | | Tube 5 | -0.02 | – | – | 0.044 | | |
| | | Tube 8 | 0.00 | – | – | 0.800 | | |
| | | s(q) | – | 3.59 | 20.36 | <0.001 | | |
| | Eggs | Intercept | 0.43 | – | – | <0.001 | 0.119 | 13.9 |
| | | Tube 5 | -0.01 | – | – | 0.551 | | |
| | | Tube 8 | 0.02 | – | – | 0.023 | | |
| | | s(q) | – | 3.59 | 6.55 | <0.001 | | |
| CV of body size | Adults | Intercept | 0.27 | – | – | <0.001 | 0.0908 | 10.6 |
| | | Tube 5 | 0.00 | – | – | 0.909 | | |
| | | Tube 8 | -0.01 | – | – | 0.351 | | |
| | | s(q) | – | 2.10 | 9.92 | <0.001 | | |
| | Q_juveniles | Intercept | 0.38 | – | – | <0.001 | 0.0648 | 8.11 |
| | | Tube 5 | -0.02 | – | – | 0.421 | | |
| | | Tube 8 | -0.08 | – | – | 0.027 | | |
| | | s(q) | – | 1.29 | 7.35 | 0.002 | | |
| | Active juveniles | Intercept | 0.32 | – | – | <0.001 | 0.315 | 32.7 |
| | | Tube 5 | 0.03 | – | – | 0.005 | | |
| | | Tube 8 | 0.02 | – | – | 0.033 | | |
| | | s(q) | – | 2.21 | 40.27 | <0.001 | | |
| | Eggs | Intercept | 0.26 | – | – | <0.001 | 0.066 | 8.29 |
| | | Tube 5 | 0.00 | – | – | 0.742 | | |
| | | Tube 8 | -0.02 | – | – | 0.070 | | |
| | | s(q) | – | 2.33 | 5.102 | 0.002 | | |
| Skewness of body size | Adults | Intercept | -0.10 | – | – | 0.136 | -0.005 | 0.746 |
| | | Tube 5 | -0.05 | – | – | 0.611 | | |
| | | Tube 8 | 0.04 | – | – | 0.669 | | |
| | | s(q) | – | 1.00 | 0.93 | 0.335 | | |
| | Q_juveniles | Intercept | -0.04 | – | – | 0.735 | -0.018 | 0.078 |
| | | Tube 5 | -0.01 | – | – | 0.946 | | |

| | | | | | | | |
|---|---|---|---|---|---|---|---|
| | Tube 8 | -0.00 | – | – | 0.973 | | |
| | s(q) | – | 1.00 | 0.12 | 0.733 | | |
| Active | Intercept | 0.14 | – | – | 0.005 | 0.0004 | 1.28 |
| juveniles | Tube 5 | 0.11 | – | – | 0.105 | | |
| | Tube 8 | 0.08 | – | – | 0.252 | | |
| | s(q) | – | 1.00 | 0.26 | 0.612 | | |
| Eggs | Intercept | -0.02 | – | – | 0.741 | -0.008 | 0.417 |
| | Tube 5 | 0.03 | – | – | 0.811 | | |
| | Tube 8 | 0.06 | – | – | 0.582 | | |
| | s(q) | – | 1.00 | 0.70 | 0.403 | | |

## Reference


1 Deere, J. A. & Smallegange, I. M. Individual differences in developmental trajectory leave a male polyphenic signature in bulb mite populations. *Peer Community Journal* **3**, doi:10.24072/pcjournal.351 (2023).